

Donor–Acceptor-Type Organic-Small-Molecule-Based Solar-Energy-Absorbing Material for Highly Efficient Water Evaporation and Thermoelectric Power Generation

Yuanyuan Cui, Jing Liu, Zhiqiang Li, Mingyang Ji, Meng Zhao, Meihua Shen, Xue Han, Tao Jia,* Chenglong Li,* and Yue Wang

Recently, owing to the great structural tunability, excellent photothermal property, and strong photobleaching resistance, organic-small-molecule photothermal materials are proposed as promising solar absorbent materials. Herein, through fusing two strong electron-withdrawing units dibenzof[*f,h*]quinoxaline and anthraquinone units, a rigid planar acceptor dibenzo[*a,c*]naphtho[2,3-*h*]phenazine-8,13-dione (PDN) with stronger electron-withdrawing ability is obtained and used to construct donor–acceptor-type organic-small-molecule solar-energy-absorbing material, 2,17-bis(diphenylamino)dibenzo[*a,c*]naphtho[2,3-*h*]phenazine-8,13-dione (DDPA-PDN). The new compound exhibits a strong intramolecular charge transfer character and conjugates rigid plane skeleton, endowing it with a broadband optical absorption from 300 to 850 nm in the solid state, favorable photothermal properties, high photothermal conversion ability, and good photobleaching resistance. Under laser irradiation at 655 nm, the solid photothermal conversion efficiency of the resulting DDPA-PDN molecule reaches 56.23%. Additionally, DDPA-PDN-loaded cellulose papers equipped with abundant microchannels for water flow are integrated with thermoelectric devices, thus achieving an evaporation rate and voltage as high as 1.07 kg m⁻² h⁻¹ and 83 mV under 1 kW m⁻² solar irradiation, respectively. This study demonstrates the application of photothermal organic-small-molecules in water evaporation and power generation, therefore offering a valuable prospect of their utilization in solar energy harvesting.

1. Introduction

As an alternative to fossil fuels, solar energy has been considered more environmentally benign and renewable,^[1] thus has aroused widespread research interest among scientists in photochemical, photovoltaic and photothermal fields.^[2–4] The excessive growth of population and concomitant demands on higher living standard lead to unprecedented requirements on fresh water, which render the traditional water purification systems relying upon fossil fuel consumption unsustainable. Therefore, it is necessary to develop eco-friendly technologies to achieve sustainable development goals.^[5–10] Photothermal conversion of solar energy has been considered as a renewable, green and pollution-free way for sustainable development, thus exerting usage in water evaporation and electricity generation without fossil fuel consumption.^[11–13] In the process of photothermal conversion, the approach of water evaporation critically affects the photothermal

conversion efficiency and evaporation rate. In recent years, interfacial evaporation becomes the primary structural guidance to construct the solar-driven water evaporation system, which consists of solar energy absorption layer (photothermal material), steam escape channel, water transportation channel and heat insulation layer.^[14–17] Accordingly, the selective heating system surface in the form of interfacial evaporation gives rise to a challenge on the feasibility of thermoelectric conversion in resolving the energy crisis. At present, it is impendent to develop efficient photothermal materials for the construction of solar energy driven water and electricity integration device.

Currently the common photothermal materials mainly involve carbon-based inorganic materials,^[18–20] metal-based inorganic materials,^[21,22] organic–polymer,^[23–25] organic–inorganic hybrid materials,^[26,27] organic cocrystals materials,^[28] and purely organic-small-molecule materials.^[29] Among them, photothermal materials comprised of organic-small-molecules have attracted growing attention due to their unique advantages in processing feasibility, structural diversity and fine-tuned properties.^[29,30–36] As solar-energy-absorbing material, organic-small-molecule photothermal material can collect waste heat to generate electricity during water evaporation, which promises

Y. Cui, C. Li, Y. Wang
State Key Laboratory of Supramolecular Structure and Materials
College of Chemistry
Jilin University
2699 Qianjin Street, Changchun 130012, P. R. China
E-mail: chenglongli@jlu.edu.cn

J. Liu, M. Zhao, M. Shen, X. Han, T. Jia
Key Laboratory of Forest Plant Ecology
Ministry of Education
Engineering Research Center of Forest Bio-Preparation
College of Chemistry
Chemical Engineering and Resource Utilization
Northeast Forestry University
26 Hexing Road, Harbin 150040, P. R. China
E-mail: jiataopolychem@nefu.edu.cn

Z. Li
Jihua Laboratory
No. 28 Island Ring South Road, Foshan 528200, P. R. China
M. Ji
Research School of Polymeric Materials
School of Materials Science and Engineering
Jiangsu University
Zhenjiang 212013, P. R. China

 The ORCID identification number(s) for the author(s) of this article can be found under <https://doi.org/10.1002/adfm.202106247>.

DOI: 10.1002/adfm.202106247

access to multifunctional devices capable of photothermal water evaporation and thermoelectric power generation simultaneously.^[18] Despite the promising prospect of organic photothermal small molecules in solar energy harvesting and conversion, further exploration is still required to broaden their absorption spectra and promote their photothermal conversion, therefore enable their utilization in high-performance water evaporation/thermoelectric devices.^[29,35] In general, organic conjugated molecules with strong electron donor–acceptor (D–A) structure can largely redshift absorption spectra by effective electron delocalization. In addition, the conjugate rigid plane structure contributes to increase the π – π stacking in the aggregate state, which can further widen absorption spectra. Even more interestingly, according to the energy-gap law,^[37–39] the resultant small energy gap could promote nonradiative decay to generate heat. Therefore, the development of organic-small-molecules with strong D–A structure and conjugate rigid plane skeleton is of crucial importance to efficiently convert solar energy to heat for high-performance water evaporation/thermoelectric devices.

Dibenzo[*f,h*]quinoxaline and anthraquinone are common electron-withdrawing groups used for constructing long-wavelength organic light-emitting materials due to their planarity, highly conjugated backbones and strong electron-withdrawing abilities.^[40,41] However, to construct organic photothermal materials with broad absorption spectra and narrow band

gap, their electron-withdrawing abilities and conjugate rigid plane skeleton are not sufficient enough. Herein, by fusing two strong dibenzo[*f,h*]quinoxaline and anthraquinone units together, a new stronger electron-accepting core, dibenzo[*a,c*]naphtho[2,3-*h*]phenazine-8,13-dione (PDN) with conjugate rigid planar skeleton, was developed. A novel organic-small-molecule, 2,17-bis(diphenylamino)dibenzo[*a,c*]naphtho[2,3-*h*]phenazine-8,13-dione (DDPA-PDN), featuring PDN as the acceptor and two diphenylamine (DPA) as the donors with strong D–A structure and conjugate rigid plane skeleton was synthesized (Figure 1a). DDPA-PDN presented a broad absorption spectrum from 300 to 850 nm in the solid state, contributing to efficient solar energy harvesting. As expected, DDPA-PDN exhibited highly efficient photothermal conversion and achieved a conversion efficiency as high as 56.23% under laser irradiation at 655 nm. In addition, under a 1 kW m⁻² solar irradiation, this organic photothermal material with D–A structure was tested as solar absorber for water evaporation to achieve an evaporation rate and efficiency as 1.07 kg m⁻² h⁻¹ and 73.98%, respectively. Given the efficient solar energy harvesting and conversion of DDPA-PDN molecule, it was employed as the solar absorber to coat the surface of thermoelectric devices. The resulting photothermal–electric power generation device, under 5 kW m⁻² solar irradiation and floating on water, produced a voltage up to 148 mV that could drive the rotation of a microfan. Finally, to maximize the utilization

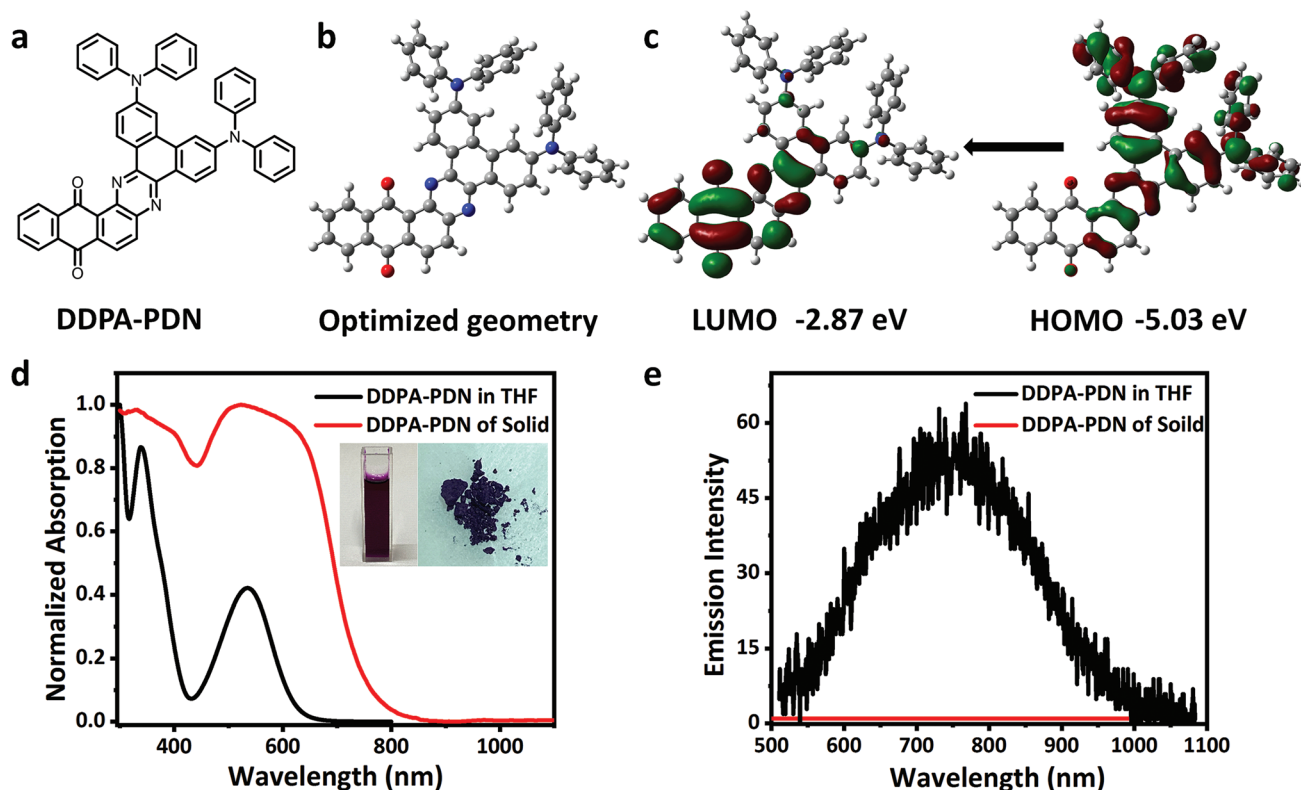
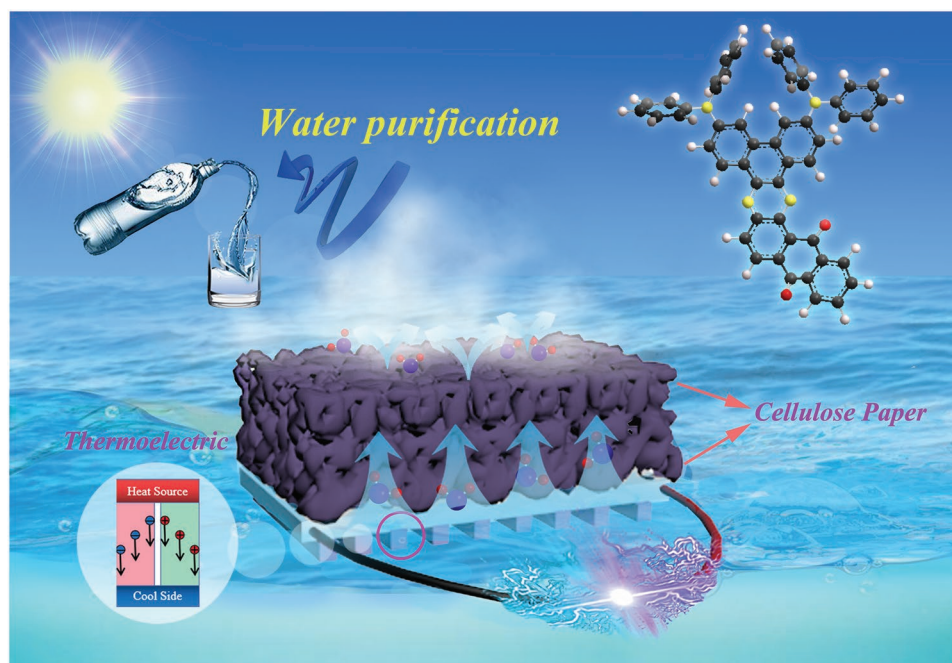


Figure 1. a) Chemical structure of DDPA-PDN. b) Optimized ground-state geometry of DDPA-PDN. c) The calculated LUMO and HOMO for DDPA-PDN. d) Normalized absorption spectra of DDPA-PDN in THF solution (10^{-5} M, calibrated with blank THF) and solid powder (calibrated with barite). Insets show the photographs of DDPA-PDN in solid powder and THF solution taken under daylight. e) Emission spectra of DDPA-PDN in THF solution (10^{-5} M) and solid powder at room temperature. Excitation wavelength (λ_{ex}) is 470 nm.



Scheme 1. Schematic diagram of water evaporation and cogeneration system.

of heat energy, a multifunctional device capable of simultaneous water evaporation and thermoelectric power generation was constructed by attaching a DDPA-PDN-loaded cellulose paper on a thermoelectric Peltier plate. With the presence of interface water evaporation within the DDPA-PDN-loaded cellulose paper, this proposed device realized a water evaporation rate of $0.89 \text{ kg m}^{-2} \text{ h}^{-1}$ and produced a stable voltage up to 43 mV as well under 1 kW m^{-2} solar irradiation (working diagram is shown in **Scheme 1**). This organic-photothermal-small-molecule with D–A structure is used in solar-driven integrated production of water and electricity combined absorber, which will be thermal evaporation and waste heat power generation technology seamless connection for practical outdoor solar desalination and electricity generation to make bold assumptions.

2. Results and Discussion

2.1. Synthesis and Characterization

The synthetic procedure of the new compound is depicted in Scheme S1 (Supporting Information). The compound was synthesized through a two-step reaction. First, the intermediate 2,17-dibromodibenzo[a,c]naphtho[2,3-h]phenazine-8,13-dione (DDPA-PD) was obtained by Pd-catalyzed Buchwald–Hartwig crossing-coupling reaction using 3,6-dibromophenanthrene-9,10-dione and DPA. Second, the target molecule DDPA-PDN was synthesized by cyclization reactions with good yield of 50%. The target product was further purified by column chromatography and the chemical structure was fully characterized by ^1H and ^{13}C NMR spectroscopy, mass spectrometry and elemental analysis. (Figures S1–S3, Supporting Information).

2.2. Thermal and Electrochemical Properties

The compound is thermodynamically and electrochemically stable. The thermal data operated by thermogravimetric analysis (TGA) and differential scanning calorimetric (DSC) measurement is collected in Table S1, Supporting Information. The TGA measurement indicates that DDPA-PDN has excellent thermal stability with high decomposition temperature (T_d , corresponding to 5% weight loss) of 447 °C. The glass transition temperature (T_g) was observed at 172 °C from the DSC measurement (Figure S4–S5, Supporting Information). The stable thermal properties reveal that this compound is suitable as photothermal material. The electrochemical property of DDPA-PDN was performed by cyclic voltammetry (CV) measurement. As shown in Figure S6 (Supporting Information), the quasireversible oxidation and reduction processes observed in dichloromethane solution are assigned to the oxidation of DPA unit and the reduction of PDN unit. Cyclic voltammogram of DDPA-PDN (Table S1, Supporting Information) shows that the highest occupied molecular orbital (HOMO) and lowest unoccupied molecular orbital (LUMO) values are -5.40 and -3.64 eV respectively, and an ideal narrow band gap value of 1.76 eV is calculated. The small band-gap makes DDPA-PDN have the ability to absorb solar energy from the full spectral range. Furthermore, the HOMO of DDPA-PDN measured by ultraviolet photoelectron spectroscopy is -5.47 eV and the LUMO level estimated from optical band gap and HOMO level is -3.67 eV, which is in agree with electrochemical measurement (Figure S6, Supporting Information).

2.3. Density Functional Theory (DFT) Calculations

First of all, in order to further understand the geometrical and electronic properties of DDPA-PDN, the ground-state

geometry of the compound and the related acceptor units were optimized in the gas phase using Gaussian 09 program package at the B3LYP/6-31g(d) level starting from the geometry obtained from the initial geometry. As shown in Figure 1b, DDPA-PDN exhibits an almost plane molecular structure, which is advantageous to increase the π - π stacking in the aggregate state, and thus further widen absorption spectra. The optimized molecular structure and the density of state distributions of HOMO and LUMO are displayed in Figure 1c. The LUMO of DDPA-PDN is mainly localized on the acceptor core while the HOMO delocalizes across the whole molecule except the anthraquinone part. The energy levels of HOMO and LUMO of the compound based on the theoretical calculations are calculated to be -5.03 and -2.87 eV and a small calculated band-gap of 2.16 eV is obtained, which is in agree with electrochemical band-gap. Additionally, the LUMO of the fused acceptor PDN is calculated to be shallower than its composition dibenzo[*f,h*]quinoxaline and anthraquinone units (Figure S7, Supporting Information), proving PDN stronger electron-accepting ability.

2.4. Photophysical Properties

The ultraviolet-visible absorption spectra of DDPA-PDN in tetrahydrofuran (THF) solution (10^{-5} M) and solid state at room temperature is shown in Figure 1d. The absorption in THF at lower wavelength region below 450 nm can be attributed to n - π^* and π - π^* transitions of the DPA, PDN moieties, while the broad low-energy absorption band from 430 to 685 nm originates from intramolecular charge transfer (ICT) transition from the donor to the acceptor. Noticeably, the aggregated state of the photothermal molecule exhibits a wide absorption spectrum from 300 to 850 nm with strong absorption peak that lays a good foundation for the efficient use of solar energy. Compared with the solution state, the absorption spectrum of the solid state behaves a significant red shift and stronger absorption intensity, which is attributed to strong intermolecular π - π stacking led by highly conjugated rigid planar skeleton.^[41] On the other hand, the emission spectra of DDPA-PDN at room temperature were captured (Figure 1e). No emission spectra in solid state and extremely weak emission spectra in THF solution (10^{-5} M) can be collected, and corresponding fluorescence quantum yields are only 0.29% and 0.08%, which indicates that the emission of DDPA-PDN can be seriously quenched and finally leads to the enhancement of nonradiative decay of molecules to generate heat. Overall, DDPA-PDN mainly leads to strong intramolecular charge transfer through the D-A structure, resulting in large electron delocalization and small band gap. Furthermore, the conjugate rigid plane structure of PDN acceptor core contributes to increase the π - π stacking in the aggregate state, which can promote exciton to be quenched and further widen absorption spectra. Thus, the energy of the excited state of DDPA-PDN is more tended to generate heat through nonradiation decay.

2.5. Photothermal Performance of DDPA-PDN

Inspired by a wide absorption spectrum and good thermal stability, the photothermal performance of DDPA-PDN solid

powder was evaluated by the rapid temperature change under the IR camera. The IR camera was applied to quickly and accurately capture the photos of the DDPA-PDN material under 0.8 W cm^{-2} illumination density, so as to better observe the temperature change of the material under 655 nm laser irradiation. In Figure 2a, it shows clearly that the temperature of DDPA-PDN material rises rapidly to about $144 \text{ }^\circ\text{C}$ within 20 s. When the temperature stable at $146 \text{ }^\circ\text{C}$ in 30 s the laser is turned off immediately, and then the temperature drops dramatically to room temperature with time. In Figure 2b, the maximum stable temperature of the 5 mg solid powder gradually increases with the increase of power density under the irradiation of 655 nm laser. When the power density is lower than 0.6 W cm^{-2} , the temperature change is slight and negligible. This is because little heat can be generated when the power density is below 0.6 W cm^{-2} , and it is easy to be dissipated through thermal conduction, thermal radiation and thermal convection processes. Therefore, it is difficult for the IR camera to capture this tiny temperature change. When the power density is 0.9 W cm^{-2} , the temperature can even reach as high as $201 \text{ }^\circ\text{C}$. The excellent photothermal performance of DDPA-PDN has been obviously proved, but it is far from enough. Notably, the organic photothermal materials used for solar energy conversion can not only lay emphasis on unexceptionable thermal stability and photothermal performance, but also understand the photobleaching resistance of the materials, so as to obtain the possibility of stable and long-term photothermal conversion.

The 5 mg DDPA-PDN powder was irradiated under 655 nm laser with a power density of 0.8 W cm^{-2} , and the optical stability was observed through the difference of temperature rise and temperature drop in five periods (Movie S1, Supporting Information). As depicted in Figure 2c, there is still about $146 \text{ }^\circ\text{C}$ under the irradiation of 0.8 W cm^{-2} laser for 2 h (Figure S8, Supporting Information), which manifests it has excellent photobleaching resistance. In addition, under the irradiation of 655 nm laser, the photothermal conversion efficiency of DDPA-PDN can be as high as 56.23% (Figure S9, Supporting Information).^[42] In a word, DDPA-PDN molecule has broad absorption spectrum from 300 to 850 nm, admirable solar energy conversion ability, excellent thermal stability, and photobleaching resistance, which is better compared with other traditional organic photothermal small molecules and expected to be a potential candidate material for solar absorbent in the process of solar-thermal conversion technology.

2.6. Photothermal Water Evaporation Capacity of DDPA-PDN

Based on the excellent photothermal property of DDPA-PDN, it is proposed in this work that DDPA-PDN can be combined with cellulose paper to produce a highly efficient solar absorber for interfacial heating and evaporating water. Cellulose paper used as floating carrier and interface evaporation of water is adopted because of its excellent light absorption performance, high water transportation performance, good heat insulation performance, high energy conversion efficiency.^[43-45] The specific creation method of cellulose paper is shown in Figure S10 (Supporting Information). Insight into their structure through

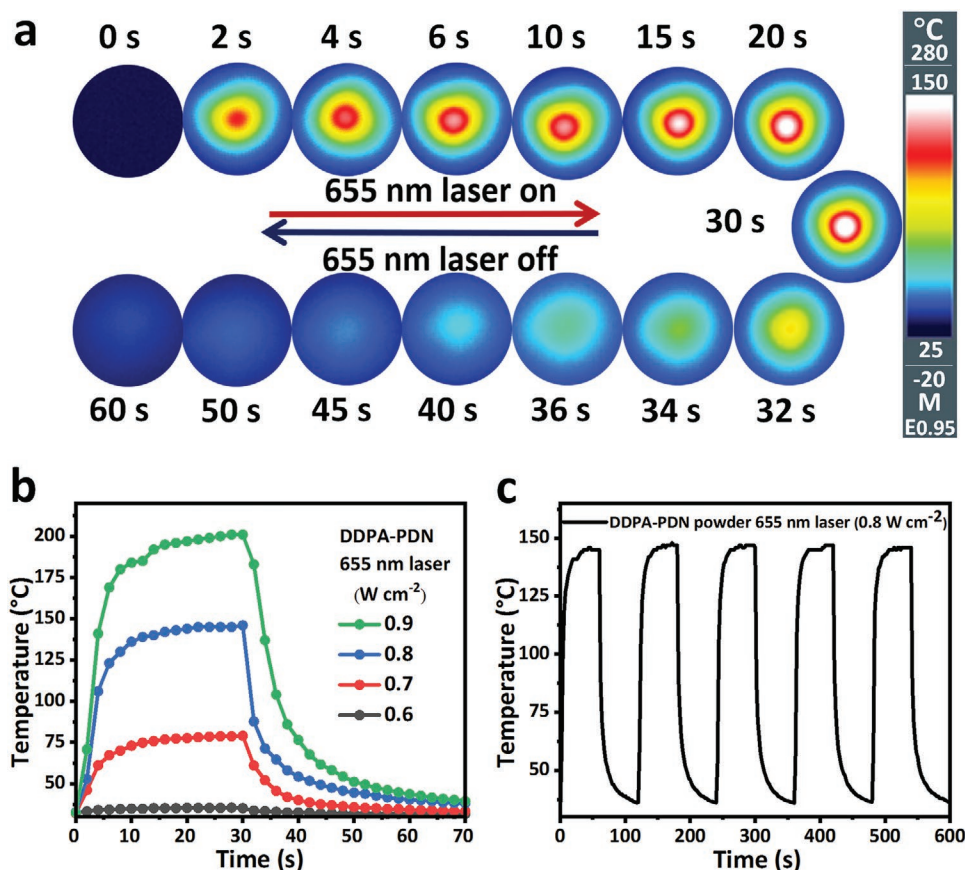


Figure 2. a) IR thermal photos of DDPA-PDN powder (5 mg) under 655 nm laser irradiation (0.8 W cm^{-2}) and then turned off at 30 s. b) Photothermal conversion behavior of DDPA-PDN powder (5 mg) under 655 nm laser irradiation at different laser powers (0.6, 0.7, 0.8, and 0.9 W cm^{-2}). c) Photobleaching resistance property of DDPA-PDN powder (5 mg) during five cycles of on-off processes.

scanning electron microscopy (SEM; **Figure 3a**) it can be observed that the surface of DDPA-PDN cellulose paper is coarser than that of blank cellulose paper, indicating that the material can be well attached to the surface of the cellulose paper, and the ideal pore structure is more conducive to the effective collection of sunlight inside the cellulose paper and the floating surface evaporation water.^[46]

Under normal air conditions, the load DDPA-PDN cellulose paper has absorption in the range of 300–850 nm, which is much higher than the blank cellulose paper (**Figure 3b**). As shown in **Figure S11** (Supporting Information), the little difference of the absorption spectrum between the powder and DDPA-PDN cellulose paper is on account of the change of sample morphology. In order to assess the photothermal conversion ability of the solar absorber (DDPA-PDN cellulose paper), the temperature change process of the paper under one sunlight intensity for 10 min was quickly recorded. It can be seen that the temperature of DDPA-PDN cellulose paper can reach up to $62 \text{ }^\circ\text{C}$ contrasting with blank cellulose paper only $37.2 \text{ }^\circ\text{C}$ under the same condition (**Figure 3c**). After long-term evaporation and impregnation, although the surface has slight change, it can still reach the temperature in the dry state (**Figure S12**, Supporting Information) and it remains relatively stable under 2 h of sunlight irradiation (**Figure S13**, Supporting Information). In addition, as shown in the insets (**Figure 3c**),

the IR thermal photos manifest that DDPA-PDN has the rapid heating process and the ideal equilibrium temperature. The special structural characteristic of DDPA-PDN makes the highest temperature of the DDPA-PDN cellulose paper almost independent of the quality (**Figure S14**, Supporting Information). In other words, compared to other organic photothermal small molecules, a little mass of the material required can reach the desired temperature. Therefore, this cellulose paper is feasible in water evaporation because of excellent photothermal conversion behavior, the characteristics of saving materials and easy synthesis.

In the next moment, the DDPA-PDN cellulose paper was evaporated by water test to verify the evaporation effect, with the basic design rationale illustrated in **Figure 3d**. The DDPA-PDN cellulose paper was placed on top of a small glass bottle filled with water and irradiated with a sunlight beam for 1 h. At the same time, the temperature change was recorded by IR thermal camera, and the mass loss of water was paid attention to at all times. As can be seen from the insets in **Figure 3e**, the photograph of DDPA-PDN cellulose paper floating on the top of water proves that at the interface, the heat transfer of internal water and cellulose paper is reduced and the evaporation efficiency is enhanced. The surface temperature of DDPA-PDN cellulose paper floating on the water is remarkably higher than blank cellulose paper, the former reaches $35.6 \text{ }^\circ\text{C}$ while

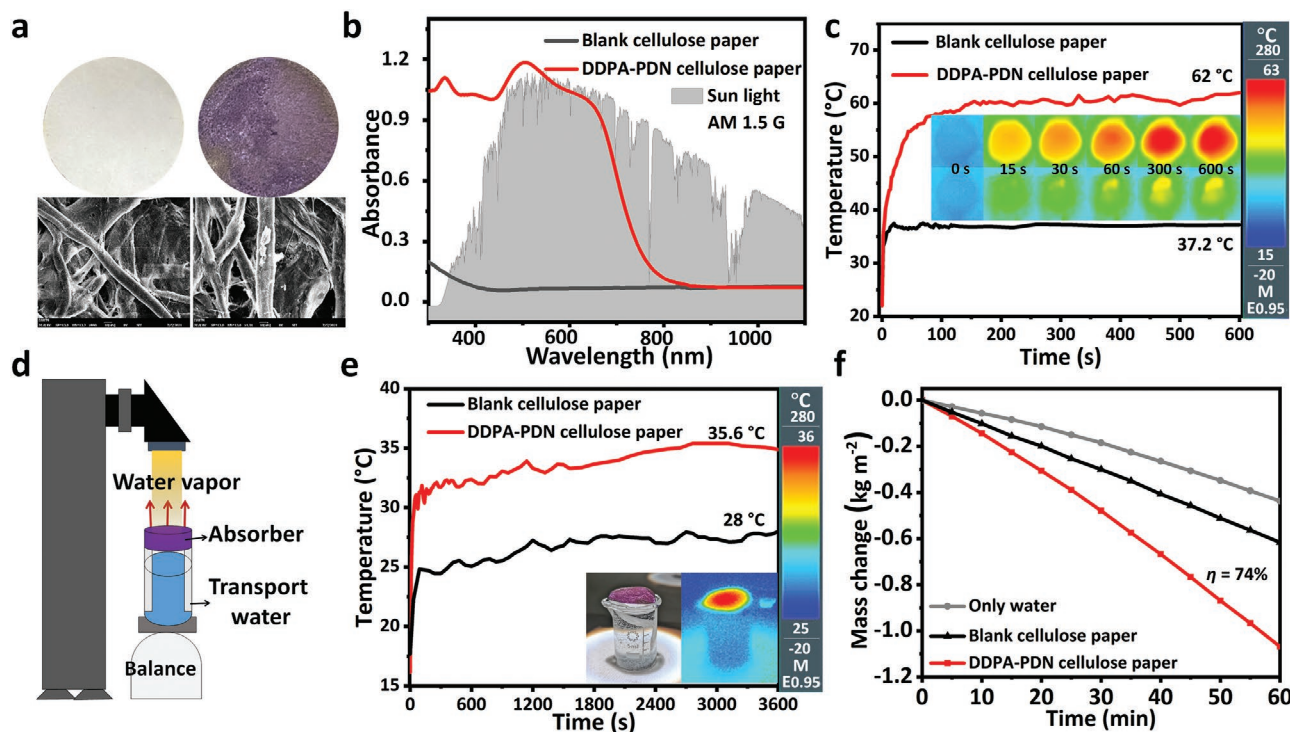


Figure 3. a) Digital photos and SEM images of blank cellulose paper and DDPA-PDN-loading cellulose paper (DDPA-PDN cellulose paper). The amount of DDPA-PDN used in preparing DDPA-PDN cellulose paper is 5 mg. b) Absorption of blank cellulose paper (calibrated with barite) and the DDPA-PDN cellulose paper (calibrated with barite), and the solar spectral irradiance (gray, AM 1.5 G). c) Photothermal conversion behavior of blank cellulose paper and the DDPA-PDN cellulose paper under 1 kW m^{-2} solar irradiation. Insets show IR thermal photos of blank cellulose paper and the DDPA-PDN cellulose paper under 1 kW m^{-2} solar irradiation. d) Solar energy driven water evaporation diagram. Room temperature is about $24 \text{ }^{\circ}\text{C}$. e) Temperature variation with time of water evaporation process for blank cellulose paper and DDPA-PDN cellulose paper under 1 kW m^{-2} solar irradiation. The inset shows an infrared thermal image of 1 kW m^{-2} solar irradiation. f) Mass loss curves of pure water evaporation (only water) and blank cellulose paper and DDPA-PDN cellulose paper within 1 h under simulated sunlight of 1 kW m^{-2} solar irradiation.

the latter only $28 \text{ }^{\circ}\text{C}$ after an hour. With the data recorded at real time, the relationship curve between water mass loss and time in 1 h shows that the evaporation efficiency of impregnated cellulose paper is much higher than that of blank water and cellulose paper (Figure 3f). Through calculation, the evaporation rate of the DDPA-PDN cellulose paper is as high as $1.07 \text{ kg m}^{-2} \text{ h}^{-1}$ compared to pure water only $0.44 \text{ kg m}^{-2} \text{ h}^{-1}$ and blank cellulose paper $0.62 \text{ kg m}^{-2} \text{ h}^{-1}$. Furthermore, the efficiency of solar-driven water evaporation (η) for DDPA-PDN cellulose paper was calculated to be as high as 73.98%. In general, the heat loss of a steam generator is divided into conduction loss, radiation loss and convection loss. In this work, we calculated the heat loss in the evaporation process according to the previous report.^[29,47] The conduction, radiation, and convection losses are estimated to be 8.5%, 2.3%, and 2.1%, respectively (Supporting Information). Due to its high photothermal conversion efficiency and excellent water evaporation rate, such solar distillation technology can provide potential opportunities for fresh water.

2.7. Photothermal–Electric Conversion Ability of DDPA-PDN

As a solar absorber, the DDPA-PDN cellulose paper can be applied to water evaporation. However, there will still be afterheat

wasted in the evaporation process. Hence, a combination system of photothermal evaporation water and afterheat utilization for power generation is envisaged, and the feasibility of thermoelectric power generation is verified by recording corresponding data. Thermoelectric devices collect electrical energy through the Seebeck effect triggered by the static temperature difference between the solar absorber and water. Photothermal water evaporation material DDPA-PDN is combined with thermoelectric device design, the heat energy can be converted into electric energy under the irradiation of sunlight and the experimental schematic design scheme is shown in Figure 4a. 20 mg of DDPA-PDN solid powder and a small amount of thermal conductive adhesive were evenly coated on the surface of the thermoelectric device to obtain the hot end temperature under simulated sunlight irradiation, while the lower part of the thermoelectric device used flowing water to obtain the cold end temperature.

The electromotive force is generated when the temperature difference between hot and cold ends is produced, and the relation of thermoelectric device output voltage with time under different solar intensity is shown in Figure 4c. Comparing blank device and the device loading DDPA-PDN solid powder in dark, it can be clearly seen that the corresponding stable voltage is higher with the increase of light density. The voltage is 83 mV under 1 kW m^{-2} solar irradiation while the stable voltage can even reach 148 mV under the irradiation of

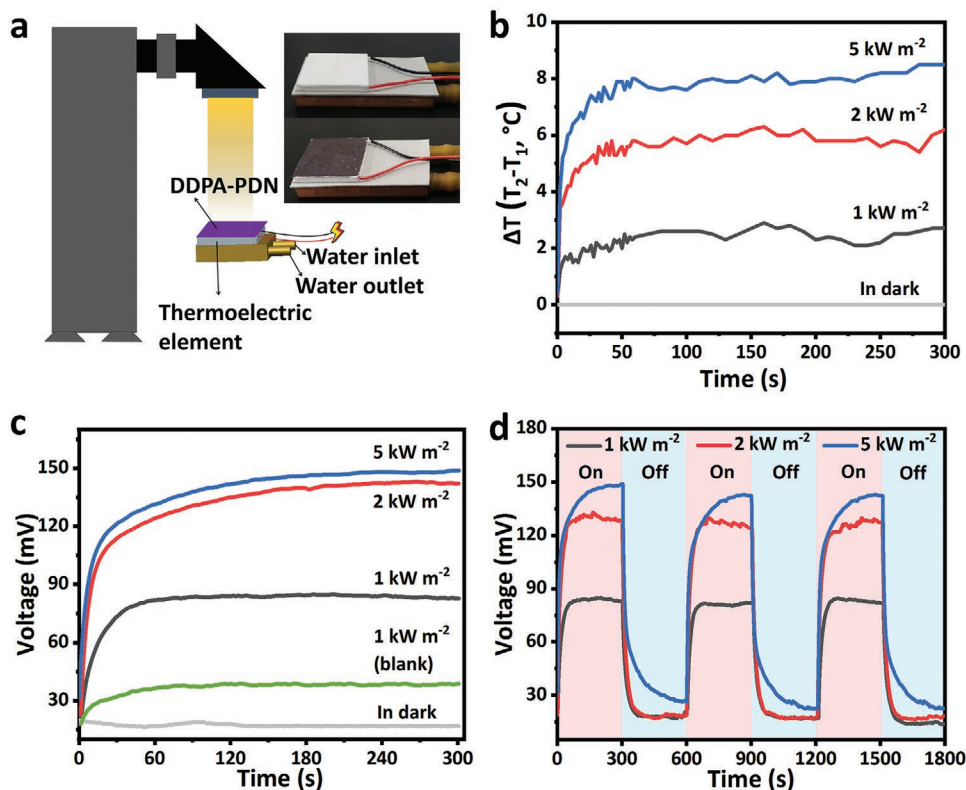


Figure 4. a) Generating design of thermoelectric device. On the right is a comparison diagram of the actual blank thermoelectric device and the thermoelectric device loaded with DDPA-PDN powder (20 mg). b) Temperature difference between the surface of a thermoelectric device and the circulating water under different light intensity (dark, 1, 2, and 5 kW m^{-2}). c) Thermoelectric conversion capability of DDPA-PDN powder (20 mg) that is attached to the surface of the thermoelectric device under different light intensities (dark, 1, 2, and 5 kW m^{-2}). d) Stabilizing thermoelectric generating property of DDPA-PDN powder (20 mg) during three cycles of on-off processes.

5 kW m^{-2} solar irradiation. Thus, it is possible to use DDPA-PDN for thermoelectric power generation. Simultaneously, we tested the voltage stability under different light intensities in three cycles (Figure 4d). The results reveal that the output voltage has certain regularity and the thermoelectric conversion is relatively stable under different illumination densities. When we simulate sunlight exposure at a high density, the device can drive a small fan to rotate quickly (Movie S2, Supporting Information). Figure 4b and Figure S15 (Supporting Information) respectively show the curves of temperature difference in the process of thermoelectric generation and cold and hot end temperature comparison diagram under different light intensities. In a word, the possibility of the photothermal material being used for thermoelectric conversion is proved and pave the way for the development of the synergistic system of photothermal evaporation and thermoelectric power generation.

2.8. The Ability to Coproduce Water and Electricity of DDPA-PDN

The possibility of photothermal evaporated water and thermoelectric power generation has been confirmed and we boldly assumed the synergistic system of photothermal evaporated water and thermoelectric power generation, which can generate water vapor under the irradiation of sunlight and generate

power with waste heat. Its design diagram and actual device are shown in Figure 5a. A polystyrene foam frame is used to fix the thermoelectric device, and the lower part of the cellulose paper is immersed in water. The fiber structure of the cellulose paper becomes an efficient water pump to transport water and forms a water evaporation layer above the thermoelectric device. When the DDPA-PDN cellulose paper is illuminated by sunlight, the upper part of the thermoelectric device reaches a higher temperature, forming a temperature difference with the lower static water as the power generation core, which can convert the waste heat into electric energy. In this way, it provides theoretical support for the combination of thermoelectric devices and photothermal materials to realize the combined generation of water and electricity. The synergistic system of evaporated water and power generation could be comprehensive evaluated by IR camera.

As shown in Figure 5c, the evaporation rate of water under coproduction can reach $0.89 \text{ kg m}^{-2} \text{ h}^{-1}$ and the evaporation efficiency is 61.06% under 1 kW m^{-2} solar irradiation,^[48,49] which is slightly lower than that of single evaporated water. Figure 5b shows the stable temperature difference of blank cellulose paper and DDPA-PDN cellulose paper by thermal imaging instrument under different solar light intensity. At 1 kW m^{-2} solar irradiation intensity, the temperature difference (ΔT) of DDPA-PDN cellulose paper is significantly higher than that of blank cellulose paper and the stable temperature difference also

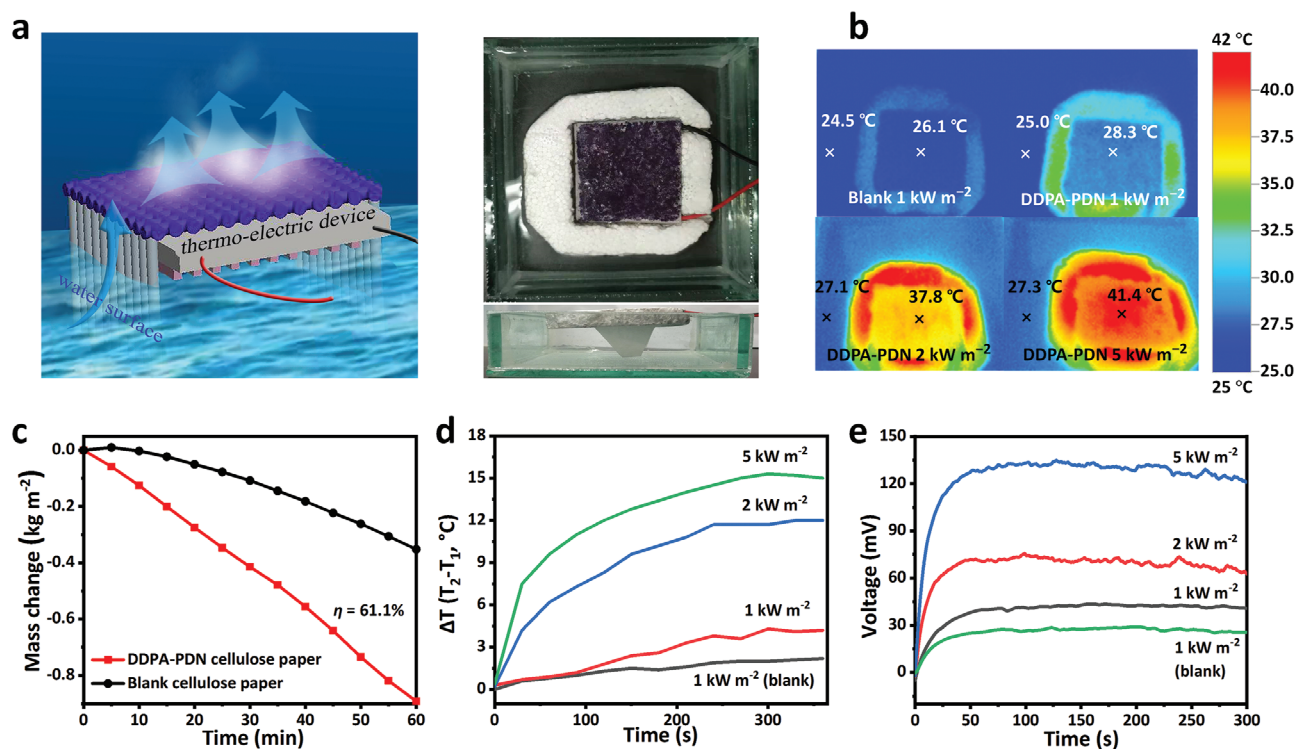


Figure 5. a) Integrated design drawing of water evaporation and thermoelectric generation. The photos on the right are the top and side views of the actual device. Among them, polystyrene foam is used as a carrying float. b) IR images of thermoelectric device surface and water under different light intensities (1, 2, and 5 kW m⁻²). c) Mass change diagram of integrated unit in 1 h. d) Temperature difference between the surface of the DDPA-PDN cellulose paper and the water under different light intensity (1, 2, and 5 kW m⁻²). e) Thermoelectric conversion capability of DDPA-PDN powder (20 mg) that is attached to the surface of cellulose paper under different light intensities (1, 2 and 5 kW m⁻²).

gradually increases with the increase of light intensity. The temperature difference causes a current to be generated in the thermoelectric device, and the current increases with the increase of the temperature difference. Figure 5d,e shows the temperature difference changes and voltage of the integrated system of water evaporation and thermoelectric generation under different light intensity, and the integrated device can reach 43 mV under 1 kW m⁻² solar irradiation. To sum up, DDPA-PDN cellulose paper has broad application prospects in water evaporation and waste heat utilization for power generation.

3. Conclusion

In summary, through fusing two strong electron-withdrawing units dibenzof[*f,h*]quinoxaline and anthraquinone units together, the rigid planar acceptor PDN with stronger electron-withdrawing ability was obtained and used to construct an organic-small-molecule solar-energy-absorbing material, DDPA-PDN. Strong ICT character and the conjugate rigid plane skeleton endow DDPA-PDN with a broadband optical absorption from 300 to 850 nm in the solid state, favorable photothermal property, high photothermal conversion ability, and good photobleaching resistance. In addition, DDPA-PDN exhibits excellent and stable photothermal behavior under 655 nm laser irradiation, with an efficiency of 56.23%. These excellent properties make the material an ideal solar absorber for solar

energy conversion. Using cellulose paper as the carrier, the photothermal water evaporation experiment was carried out, and DDPA-PDN exhibits stable photothermal behaviors with a high efficiency of 73.98% under 1 kW m⁻² solar irradiation. At the same time, thermoelectric devices were employed as carrier to make full use of waste heat for power generation. The voltages reach up to 83 mV for flowing water under the light of 1 kW m⁻² solar irradiation and it even drive a small fan at high solar exposure density. Moreover, the integrated device of water evaporation and waste heat power generation designed by us can reach 0.89 kg m⁻² h⁻¹ under 1 kW m⁻² solar irradiation. In short, the admirable performance of the material will contribute to the efficient use of solar thermal conversion and become a new step for the combination of water evaporation and power generation synergies.

4. Experimental Section

All reagents and solvents were obtained from Energy Chemical Co. and J&K scientific Ltd. Co. and used as received without further purification. All reactions were carried out using Schlenk technique under nitrogen atmosphere.

Synthesis of 3,6-Bis(diphenylamino)phenanthrene-9,10-dione (DDPA-PD): A mixture of 3,6-dibromophenanthrene-9,10-dione (3.66 g, 10 mmol), diphenylamine (4.22 g, 25 mmol), tris(dibenzylideneacetone) dipalladium(0) (Pd₂(dba)₃) (275 mg, 0.3 mmol), cesium carbonate (Cs₂CO₃) (13.04 g, 40 mmol), 1.0 M solution of tri-*tert*-butyl phosphine (P(*t*-Bu)₃) in toluene (3 mL) and toluene (100 mL) was stirred at 110 °C for 24 h

under nitrogen atmosphere. The mixture was cooled to room temperature and distilled water (20 mL) was added to quench the reaction. The mixture was then extracted with dichloromethane, and the combined organic solvent was dried over anhydrous sodium sulfate and removed under reduced pressure. The residue was purified by column chromatography using dichloromethane as the eluent to give a deep-red solid (2.71 g). Yield: 50%. ¹H NMR (500 MHz, DMSO-*d*₆) δ 7.86 (d, *J* = 8.7 Hz, 2H), 7.40 (t, *J* = 7.6 Hz, 8H), 7.29 (t, *J* = 7.4 Hz, 4H), 7.20 (d, *J* = 7.8 Hz, 6H), 6.79–6.73 (m, 4H), 5.75 (s, 2H). ESI-MS [M]⁺ *m/z*: 543.18 (calcd: 542.64).

Synthesis of 2,17-Bis(diphenylamino)dibenzo[*a,c*]naphtho[2,3-*h*]phenazine-8,13-dione (DDPA-PDN): A mixture of DDPA-PD (2.17 g, 4 mmol), 5,6-diamino-4a,9a-dihydroanthracene-9,10-dione (4.80 g, 20 mmol) and acetic acid (30 mL) was stirred at 120 °C for 12 h under nitrogen atmosphere. The mixture was cooled to room temperature and poured into water (100 mL). After filtered, the filter cake was dissolved in dichloromethane and dried over anhydrous sodium sulfate and removed under reduced pressure. The residue was purified by column chromatography using dichloromethane as the eluent to give a deep-red solid (1.49 g). Yield: 50%. ¹H NMR (400 MHz, Methylene Chloride-*d*₂) δ 9.07 (d, *J* = 8.8 Hz, 1H), 8.93 (d, *J* = 8.9 Hz, 1H), 8.48 (d, *J* = 8.8 Hz, 1H), 8.38 (d, *J* = 8.8 Hz, 1H), 8.22 (td, *J* = 7.1, 1.7 Hz, 2H), 7.81–7.73 (m, 2H), 7.45 (d, *J* = 2.3 Hz, 2H), 7.33 (ddd, *J* = 8.8, 7.1, 1.6 Hz, 9H), 7.26 (dd, *J* = 8.9, 2.2 Hz, 1H), 7.22–7.16 (m, 12H). ¹³C NMR (101 MHz, Chloroform-*d*) δ 183.88, 183.62, 151.01, 150.83, 146.64, 146.52, 145.21, 143.96, 142.79, 139.34, 135.38, 134.96, 134.74, 134.41, 134.14, 133.49, 133.33, 132.27, 129.67, 129.60, 129.39, 128.89, 128.70, 128.08, 127.27, 126.57, 125.90, 125.77, 125.57, 124.72, 124.54, 123.83, 122.73, 122.17, 121.30, 113.53. ESI-MS [M]⁺ *m/z*: 744.61 (calcd: 744.25). Anal. Calcd (%) for C₅₂H₃₂N₄O₂: C, 83.85; H, 4.33; N, 7.52; O, 4.30. Found: C, 84.42; H, 4.59; N, 7.46.

Supporting Information

Supporting Information is available from the Wiley Online Library or from the author.

Acknowledgements

Y.C. and J.L. contributed equally to this work. This work was supported by the National Natural Science Foundation of China (51803069), Heilongjiang Province Returnees Merit Subsidize Project (2017QD0052), China Postdoctoral Science Foundation (2018M631892), and the Science and Technology Research Project of the Education Department of Jilin Province, China (JJKH20211043K).

Conflict of Interest

The authors declare no conflict of interest.

Data Availability Statement

Research data are not shared.

Keywords

donor–acceptor structures, organic-small-molecule photothermal materials, solar–thermal conversion, thermoelectric power generation, water evaporation

Received: June 29, 2021
Revised: August 16, 2021
Published online:

- [1] a) N. S. Lewis, D. G. Nocera, *Proc. Natl. Acad. Sci. USA* **2006**, *103*, 15729; b) S. Chu, A. Majumdar, *Nature* **2012**, *488*, 294; c) Y.-L. He, Y. Qiu, K. Wang, F. Yuan, W.-Q. Wang, M.-J. Li, J.-Q. Guo, *Energy* **2020**, *198*, 117373.
- [2] a) S. U. Khan, M. Al-Shahry, W. B. Ingler, Jr., *Science* **2002**, *297*, 2243; b) X. Wang, K. Maeda, A. Thomas, K. Takanebe, G. Xin, J. M. Carlsson, K. Domen, M. Antonietti, *Nat. Mater.* **2009**, *8*, 76; c) S. Linic, P. Christopher, D. B. Ingram, *Nat. Mater.* **2011**, *10*, 911.
- [3] a) A. Kojima, K. Teshima, Y. Shirai, T. Miyasaka, *J. Am. Chem. Soc.* **2009**, *131*, 6050; b) Y. Liang, Z. Xu, J. Xia, S. T. Tsai, Y. Wu, G. Li, C. Ray, L. Yu, *Adv. Mater.* **2010**, *22*, E135; c) M. Jeong, I. W. Choi, E. M. Go, Y. Cho, M. Kim, B. Lee, S. Jeong, Y. Jo, H. W. Choi, J. Lee, J. H. Bae, S. K. Kwak, D. S. Kim, C. Yang, *Science* **2020**, *369*, 1615.
- [4] a) C. Chen, Y. Kuang, L. Hu, *Joule* **2019**, *3*, 683; b) Z. Zheng, H. Li, X. Zhang, H. Jiang, X. Geng, S. Li, H. Tu, X. Cheng, P. Yang, Y. Wan, *Nano Energy* **2020**, *68*, 104298; c) G. Liu, T. Chen, J. Xu, G. Li, K. Wang, *J. Mater. Chem. A* **2020**, *8*, 513.
- [5] N. L. Panwar, S. C. Kaushik, S. Kothari, *Renewable Sustainable Energy Rev.* **2011**, *15*, 1513.
- [6] Z. Wang, C. Yang, T. Lin, H. Yin, P. Chen, D. Wan, F. Xu, F. Huang, J. Lin, X. Xie, M. Jiang, *Adv. Funct. Mater.* **2013**, *23*, 5444.
- [7] S. Chu, Y. Cui, N. Liu, *Nat. Mater.* **2016**, *16*, 16.
- [8] C. P. Grey, J. M. Tarascon, *Nat. Mater.* **2016**, *16*, 45.
- [9] S. E. Hosseini, M. A. Wahid, *Renewable Sustainable Energy Rev.* **2016**, *57*, 850.
- [10] J. H. Montoya, L. C. Seitz, P. Chakthranont, A. Vojvodic, T. F. Jaramillo, J. K. Norskov, *Nat. Mater.* **2016**, *16*, 70.
- [11] X. Li, J. Li, J. Lu, N. Xu, C. Chen, X. Min, B. Zhu, H. Li, L. Zhou, S. Zhu, T. Zhang, J. Zhu, *Joule* **2018**, *2*, 1331.
- [12] Y. Shi, R. Li, L. Shi, E. Ahmed, Y. Jin, P. Wang, *Adv. Sustainable Syst.* **2018**, *2*, 1700145.
- [13] M. Gao, L. Zhu, C. K. Peh, G. W. Ho, *Energy Environ. Sci.* **2019**, *12*, 841.
- [14] H. Ghasemi, G. Ni, A. M. Marconnet, J. Loomis, S. Yerci, N. Miljkovic, G. Chen, *Nat. Commun.* **2014**, *5*, 4449.
- [15] Y. Ito, Y. Tanabe, J. Han, T. Fujita, K. Tanigaki, M. Chen, *Adv. Mater.* **2015**, *27*, 4302.
- [16] Y. Pang, J. Zhang, R. Ma, Z. Qu, E. Lee, T. Luo, *ACS Energy Lett.* **2020**, *5*, 437.
- [17] P. Sun, W. Zhang, I. Zada, Y. Zhang, J. Gu, Q. Liu, H. Su, D. Pantelic, B. Jelenkovic, D. Zhang, *ACS Appl. Mater. Interfaces* **2020**, *12*, 2171.
- [18] a) P. Zhang, J. Li, L. Lv, Y. Zhao, L. Qu, *ACS Nano* **2017**, *11*, 5087; b) L. Cui, P. Zhang, Y. Xiao, Y. Liang, H. Liang, Z. Cheng, L. Qu, *Adv. Mater.* **2018**, *30*, 1706805; c) L. Zhu, T. Ding, M. Gao, C. K. N. Peh, G. W. Ho, *Adv. Energy Mater.* **2019**, *9*, 1900250.
- [19] a) X. Hu, W. Xu, L. Zhou, Y. Tan, Y. Wang, S. Zhu, J. Zhu, *Adv. Mater.* **2017**, *29*, 1604031; b) G. Wang, Y. Fu, A. Guo, T. Mei, J. Wang, J. Li, X. Wang, *Chem. Mater.* **2017**, *29*, 5629.
- [20] a) Z. C. Xiong, Y. J. Zhu, D. D. Qin, F. F. Chen, R. L. Yang, *Small* **2018**, *14*, 1803387; b) L. Zhu, M. Gao, C. K. N. Peh, X. Wang, G. W. Ho, *Adv. Energy Mater.* **2018**, *8*, 1702149; c) Y. Lu, T. Dai, D. Fan, H. Min, S. Ding, X. Yang, *Sci. Bull.* **2020**, *8*, 2000567.
- [21] a) C. Zhang, C. Yan, Z. Xue, W. Yu, Y. Xie, T. Wang, *Small* **2016**, *12*, 5320; b) L. Zhou, Y. Tan, J. Wang, W. Xu, Y. Yuan, W. Cai, S. Zhu, J. Zhu, *Nat. Photonics* **2016**, *10*, 393.
- [22] R. Li, L. Zhang, L. Shi, P. Wang, *ACS Nano* **2017**, *11*, 3752.
- [23] a) Q. Chen, Z. Pei, Y. Xu, Z. Li, Y. Yang, Y. Wei, Y. Ji, *Chem. Sci.* **2018**, *9*, 623; b) P. Mu, W. Bai, Z. Zhang, J. He, H. Sun, Z. Zhu, W. Liang, A. Li, *J. Mater. Chem. A* **2018**, *6*, 18183.
- [24] a) C. Li, D. Jiang, B. Huo, M. Ding, C. Huang, D. Jia, H. Li, C. Y. Liu, J. Liu, *Nano Energy* **2019**, *60*, 841; b) X. Wang, Q. Liu, S. Wu, B. Xu, H. Xu, *Adv. Mater.* **2019**, *31*, 1807716; c) X. Zhou, F. Zhao, Y. Guo, B. Rosenberger, G. Yu, *Sci. Adv.* **2019**, *5*, eaaw5484.

- [25] S. Wang, S. Li, J. Xiong, Z. Lin, W. Wei, Y. Xu, *Chem. Commun.* **2020**, 56, 7399.
- [26] a) L. Chen, D. Li, Y. Wang, C. Duan, *Nanoscale* **2019**, *11*, 11121; b) Q. Ma, P. Yin, M. Zhao, Z. Luo, Y. Huang, Q. He, Y. Yu, Z. Liu, Z. Hu, B. Chen, H. Zhang, *Adv. Mater.* **2019**, *31*, 1808249.
- [27] a) B. Lu, Y. Chen, P. Li, B. Wang, K. Mullen, M. Yin, *Nat. Commun.* **2019**, *10*, 767; b) Y. Lu, D. Liu, Y. J. Lin, G. X. Jin, *Chem. Sci.* **2020**, *11*, 11509; c) J. Su, N. Xu, R. Murase, Z. M. Yang, D. M. D'Alessandro, J. L. Zuo, J. Zhu, *Angew. Chem., Int. Ed.* **2021**, *60*, 4789.
- [28] a) Y. Wang, W. Zhu, W. Du, X. Liu, X. Zhang, H. Dong, W. Hu, *Angew. Chem., Int. Ed.* **2018**, *57*, 3963; b) S. Tian, Z. Huang, J. Tan, X. Cui, Y. Xiao, Y. Wan, X. Li, Q. Zhao, S. Li, C.-S. Lee, *ACS Energy Lett.* **2020**, *5*, 2698; c) D. Wang, X. Kan, C. Wu, Y. Gong, G. Guo, T. Liang, L. Wang, Z. Li, Y. Zhao, *Chem. Commun.* **2020**, 56, 5223.
- [29] G. Chen, J. Sun, Q. Peng, Q. Sun, G. Wang, Y. Cai, X. Gu, Z. Shuai, B. Z. Tang, *Adv. Mater.* **2020**, *32*, 1908537.
- [30] a) B. P. Rand, J. Genoe, P. Heremans, J. Poortmans, *Prog. Photovoltaics* **2007**, *15*, 659; b) S. Loser, C. J. Bruns, H. Miyauchi, R. P. Ortiz, A. Facchetti, S. I. Stupp, T. J. Marks, *J. Am. Chem. Soc.* **2011**, *133*, 8142.
- [31] H. N. Tian, X. C. Yang, R. K. Chen, R. Zhang, A. Hagfeldt, L. C. Sun, *J. Phys. Chem. C* **2008**, *112*, 11023.
- [32] W. Zhu, Y. Wu, S. Wang, W. Li, X. Li, J. Chen, Z.-s. Wang, H. Tian, *Adv. Funct. Mater.* **2011**, *21*, 756.
- [33] a) Y. Lin, Y. Li, X. Zhan, *Chem. Soc. Rev.* **2012**, *41*, 4245; b) J. Roncali, P. Leriche, P. Blanchard, *Adv. Mater.* **2014**, *26*, 3821.
- [34] K. Cnops, B. P. Rand, D. Cheyns, B. Verreert, M. A. Empl, P. Heremans, *Nat. Commun.* **2014**, *5*, 3406.
- [35] Q. Zhang, Y. Sun, W. Xu, D. Zhu, *Adv. Mater.* **2014**, *26*, 6829.
- [36] W. Zhao, S. Li, H. Yao, S. Zhang, Y. Zhang, B. Yang, J. Hou, *J. Am. Chem. Soc.* **2017**, *139*, 7148.
- [37] R. Englman, J. Jortner, *Mol. Phys.* **1970**, *18*, 145.
- [38] J. V. Caspar, E. M. Kober, B. P. Sullivan, T. J. Meyer, *J. Am. Chem. Soc.* **1982**, *104*, 630.
- [39] T. Yang, Z. Cheng, Z. Li, J. Liang, Y. Xu, C. Li, Y. Wang, *Adv. Funct. Mater.* **2020**, *30*, 2002681.
- [40] a) H. Deol, G. Singh, M. Kumar, V. Bhalla, *J. Org. Chem.* **2020**, *85*, 11080; b) D. N. Kanekar, S. Chacko, R. M. Kamble, *New J. Chem.* **2020**, *44*, 3278.
- [41] a) Q. Zhang, H. Kuwabara, W. J. Potscavage Jr., S. Huang, Y. Hatae, T. Shibata, C. Adachi, *J. Am. Chem. Soc.* **2014**, *136*, 18070; b) A. M. Shaikh, S. Chacko, R. M. Kamble, *ChemistrySelect* **2017**, *2*, 7620.
- [42] S. W. D. Turner, N. Voisin, J. Fazio, D. Hua, M. Jourabchi, *Nat. Commun.* **2019**, *10*, 8.
- [43] a) F. Jiang, H. Liu, Y. Li, Y. Kuang, X. Xu, C. Chen, H. Huang, C. Jia, X. Zhao, E. Hitz, Y. Zhou, R. Yang, L. Cui, L. Hu, *ACS Appl. Mater. Interfaces* **2018**, *10*, 1104; b) S. Cao, P. Rathi, X. Wu, D. Ghim, Y. S. Jun, S. Singamaneni, *Adv. Mater.* **2020**, 2000922.
- [44] a) B. Hou, Z. Cui, X. Zhu, X. Liu, G. Wang, J. Wang, T. Mei, J. Li, X. Wang, *Mater. Chem. Phys.* **2019**, *222*, 159; b) L. Chen, H. Wang, S. Kuravi, K. Kota, Y. H. Park, P. Xu, *Desalination* **2020**, *483*, 114412.
- [45] a) X. Lin, M. Yang, W. Hong, D. Yu, X. Chen, *Front. Mater.* **2018**, *5*, 74; b) M. Z. Tariq, Z. Hanif, M. La, D. Choi, S. J. Park, *Int. J. Energy Res.* **2020**, *45*, 6395.
- [46] W. Li, Z. Li, K. Bertelsmann, D. E. Fan, *Adv. Mater.* **2019**, *31*, 1900720.
- [47] G. Chen, N. Zhang, N. Li, L. Yu, X. Xu, *Adv. Mater. Interfaces* **2019**, *7*, 1901715.
- [48] H. Li, Y. He, Y. Hu, X. Wang, *ACS Appl. Mater. Interfaces* **2018**, *10*, 9362.
- [49] P. Mu, Z. Zhang, W. Bai, J. He, H. Sun, Z. Zhu, W. Liang, A. Li, *Adv. Energy Mater.* **2019**, *9*, 1802158.